ACS APPLIED MATERIALS & INTERFACES

Research Article

www.acsami.org

Exciton Dynamics of CdS Thin Films Produced by Chemical Bath Deposition and DC Pulse Sputtering

Jason K. Cooper,[†] Jinbo Cao,*[,‡] and Jin Z. Zhang*[,†]

[†]Department of Chemistry and Biochemistry, University of California, Santa Cruz, California 95064, United States

[‡]Electric Materials & Physics Laboratory, GE Global Research, Energy Storage & Conversion Materials, 1 Research Circle, K1-3D1C, Niskayuna, New York 12309, United States

Supporting Information

ABSTRACT: Exciton dynamics of CdS films have been investigated using ultrafast laser spectroscopy with an emphasis on understanding defect-related recombination. Two types of CdS films were deposited on glass substrates via direct current pulse sputtering (DCPS) and chemical bath deposition (CBD) techniques. The films displayed distinct morphological, optical, and structural properties. Their exciton and charge carrier dynamics within the first 1 ns following photoexcitation were characterized by femotosecond pump probe spectroscopy. A singular value decomposition (SVD) global fitting technique was employed to extract the lifetime and wavelength dependence of transient species. The excited electrons of the DCPS sample decays through 1.8, 8, 65, and 450 ps time constants which were attributed to donor level electron trapping, valence band (VB) → conduction band (CB) recombination, shallow donor recombination, and deep donor recombination, respectively. The CBD sample shows time constants of 6, 65, and 450 ps which were attributed to CB → VB recombination, sulfur vacancy (V_S) recombination, and V_S → oxygen interstitial (O_i) donor−acceptor pair (DAP) recombination, respectively. It was found that the DCPS deposition technique produces films with lower defect density and improved carrier dynamics, which are important for high performance solar cell applications.

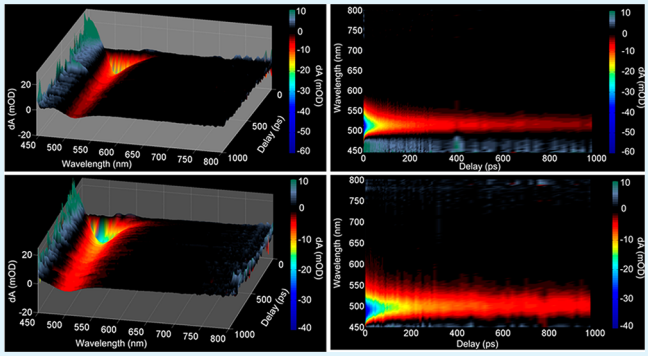

KEYWORDS: *dynamics, CdTe, CIGS, CdS, time-resolved, transient absorption*

1. INTRODUCTION

CdTe and CIGS (copper indium gallium diselenide) thin film solar cells are attractive candidates for solar photovoltaic application owing to their low production costs and relatively high conversion efficiency. For example, Empa's Laboratory for Thin Film and Photovoltaics has set a 20.4% world record efficiency for CIGS solar cells.[1] In both CdTe and CIGS systems, the *p*−*n* junction is formed between the *n*-type CdS window layer and *p*-type absorber layer. Fabrication of these layers has been an area of intensive research. Common methods of depositing the CdS layer include the use of chemical bath deposition (CBD),[2] sputtering,[3] electrochemical,[4] close space sublimation (CSS),[2] laser ablation,[5,6] vapor transport,[7] and spray pyrolysis,[8] among others. The intrinsic defect density produced by these techniques is an important factor for device performance and has been a major focus in the research field.

The native defects of CdS have been extensively studied by low temperature photoluminescence (PL)[9] for a variety of synthesis and treatment methodologies, including close space sublimation (CSS),[10,11] laser ablation,[11] chemical bath deposition (CBD),[10−13] and sputtering.[11,14] As-grown close space sublimation (CSS) films have a dominant yellow PL band from 2.07 to 2.18 eV related to donor−acceptor pair (DAP) recombination between cadmium interstitials (Cd_i) or sulfur vacancies (V_S) donor and an impurity acceptor.[10] CBD films are reported to have a red PL band between 1.59 and 2.00 eV due to surface states and V_S.[10] DAP recombination in CBD films have also been reported to be 2.349 eV.[13] V_S^{2+} has been reported to exist 2.175 eV above the valence band edge (E_v + 2.175 eV) with Cd_i^+ and sulfur interstitials (S_i^-) found at E_v + 2.012 eV and E_c − 2.275 eV, respectively.[13,15] CBD prepared films are also reported to be dominated by red emission at 1.72 eV related to V_S while RF-sputtering produced films with increased Cd_i identified by PL from 2.10 to 2.40 eV.[11] Additionally, positron annihilation spectroscopy (PAS) has identified Cd vacancies (V_{Cd}) in CBD crystals[16] as well as clustered neutral defects.[17]

Doping of CdS has also been studied in which acceptor dopants are added in an effort to produce a *p*-type material. Inadvertent doping with oxygen during CBD deposition is common, is often not addressed or characterized in the literature, but can reach values of 12%.[18−20] CBD films were found to contain an atom percent ratio of Cd:S:O of

Received: May 15, 2013
Accepted: June 24, 2013
Published: June 24, 2013

   dx.doi.org/10.1021/am4018362 | ACS Appl. Mater. Interfaces 2013, 5, 7544−7551

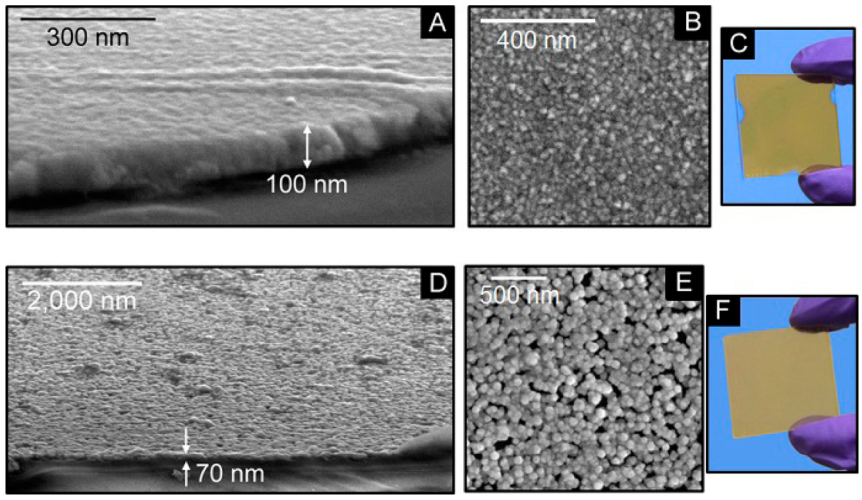

Figure 1. Sample morphology of CdS films deposited by DC pulse sputtering (DCPS), top, and chemical bath deposition (CBD), bottom. A/D: SEM image at 74° tilt angle, 150 000× magnification (A) and 20 000× magnification (D). B/E: SEM image perpendicular to the substrate, 120 000× magnification (B) and 50 000× magnification (E). C/F: Photos of CdS coated glass slides collected against a white background, digitally altered to blue to improve contrast.

45.7:42.5:11.8 by X-ray photoelectron spectroscopy (XPS).[20] Substitutional oxygen (O@S) was studied by density functional theory (DFT), but the oxygen 2p states did not alter the bandgap of CdS.[21] Other studies have found similar results in that substitutional oxygen is electrically inactive;[22] however, oxygen defects have been characterized as acceptor states at E_V + 116 meV when added to CdS by ion implantation.[23,24] The presence of oxygen can also influence intrinsic defect formation[25] as well as crystalline grain size and optical absorption energy.[26] In the case of ZnSe, oxygen is suggested to dope the lattice interstitially, breaking the Zn−Se bond to attach to the Zn and thereby causing a Se dangling bond.[22]

Herein, we have examined two CdS thin film deposition methods, CBD and DC pulsed sputtering (DCPS), for the fabrication of CdS window layers for solid state solar cell applications. Characterization of the physical morphology and crystallinity of the as-deposited films was accomplished by scanning electron microscoy (SEM) and X-ray diffraction (XRD). The ultrafast exciton dynamics of photoexcited charge carriers in the two materials was characterized by femtosecond pump probe spectroscopy. Data analysis using the technique of singular value decomposition (SVD) global fitting was employed to obtain the lifetime and wavelength dependence of the various recombination mechanisms of the exciton. The results are discussed in the context of defect related recombination and comparisons are drawn between the two deposition methods. Insights gained from these studies are important for developing improved semiconductor thin films for solar energy conversion and other photonics applications.

2. EXPERIMENTAL SECTION

2.1. Sample Preparation. *2.1.1. DC-Pulse Sputtering.* The sputtered film was prepared by applying direct current pulses to a CdS target. The deposition was carried out in an argon atmosphere at 10 mTorr and 500 W. The bipolar asymmetric pulsed direct current power was 100 kHz, and the reverse time was 3 μs.

2.1.2. Chemical Bath Deposition. CBD CdS film was deposited through a heterogeneous reaction on a glass substrate. The reactants were comprised of cadmium acetate, ammonium acetate, ammonium hydroxide, and thiourea. The temperature of the solution was maintained at 92 °C, and the reactants were continuously stirred at 400 rpm. The deposition time was 20 min, after which the substrate was rinsed with DI water, dried by spinning, and baked on a hot plate for 10 min at 110 °C.

2.2. Optical and Morphological Characterization. *2.2.1. Optical and Morphological Characterization of CdS Thin Films.* Absorption spectra were collected of the CdS thin films with a Hewlett-Packard 845A diode array UV−visible spectrometer. A FEI Quanta 3D FEG Dualbeam scanning electron microscope was used to image the two films. The films were ground with copper tape and imaged with an accelerating voltage of 5 kV, a current of 11.8 pA, and a working distance between 9 and 11 mm. Grazing incidence X-ray diffraction was collected of the thin films using a Rigaku SmartLab X-ray diffractometer with a Cu−Kα source (0.0100 degrees step, 3.0000 deg min^{-1} scan speed). The sample diffraction spectra were compared to the ICDD PDF-2/Release 2011 database for peak identification.

2.2.2. Transient Absorption Spectroscopy. Ultrafast transient absorption pump−probe spectroscopy was conducted with a Quantronix laser system consisting of a Palitra-FS optical parametric amplifier pumped by an Integra-C Ti:Sapphire amplifier system. This system has been described in detail elsewhere.[27] Briefly, 795 nm, 820 mW, and 150 fs pulses from Integra-C were split 9:1 between an optical parametric amplifier (OPA) and sapphire crystal, respectively. A white light continuum from 450 to 800 nm was generated in the sapphire crystal. The OPA was tuned to 460 nm (2.7 eV) and attenuated with neutral density (ND) filters to probe the samples at five different excitation intensities, which were 707, 220, 86, 46, and 24 nJ/pulse for the DCPS sample and 890, 195, 86, 54, and 20 nJ/pulse for the CBD sample. The differential absorption (dA) spectrum was collected over a pump probe delay period of 1000 ps consisting of average forward (−2 → 1000 ps) and reverse (1000 → −2 ps) scans where 400 spectra were averaged per data point.

The TA spectra were analyzed with singular value decomposition (SVD) global fitting (GF) procedures written in-house for Matlab, the method of which has been previously described.[28] To confirm and support SVD-GF results, single wavelength fitting for the DCPS and CBD samples was done at 510 and 490 nm, respectively.

3. RESULTS AND DISCUSSION

3.1. Sample Morphology. The CdS thin film sample morphology was analyzed with SEM for both the DCPS and CBD deposition techniques, representative images were reported in Figure 1A−C and D−F, respectively. The DCPS CdS film thickness was 100 nm and was uniformly spread across the glass surface as a dense smooth coating made up of small (20−30 nm) grains roughly spherical in shape, as

dx.doi.org/10.1021/am4018362 | ACS Appl. Mater. Interfaces 2013, 5, 7544−7551

determined by a perpendicular view of the films surface. The CBD sample was approximately 70 nm thick and was made up of more loosely packed globular to spherically shaped grains roughly 60−80 nm in size. Also seen were larger, loosely scattered grains on the order of 160−250 nm.

The crystallinity of the films was characterized using grazing incidence X-ray diffraction for the DCPS and CBD thin films, Figure 2. The DCPS sample was hexagonal and the CBS

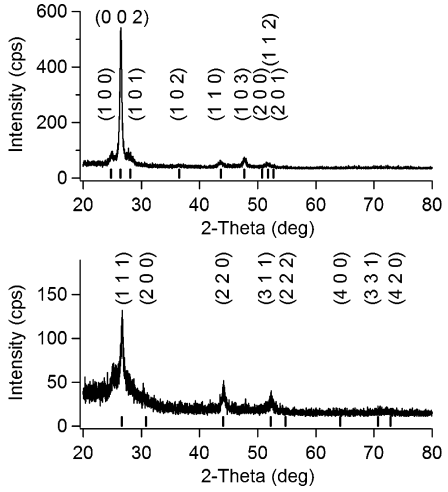

Figure 2. Grazing incidence X-ray diffraction of DCPS (top) and CBD (bottom) deposited CdS thin films on glass. Reference diffraction peaks are shown as short vertical lines, and Miller indices are provided for observed diffraction peaks.

sample was cubic. In addition, the DCPS had increased crystallinity compared to the CBD sample as evidenced by the sharp and intense (002) peak.

3.2. UV−vis Spectroscopy. The absorption spectra of the CdS thin films deposited by DC-PS and CBD were reported in Figure 3. Both samples have a first exciton peak at 486 nm

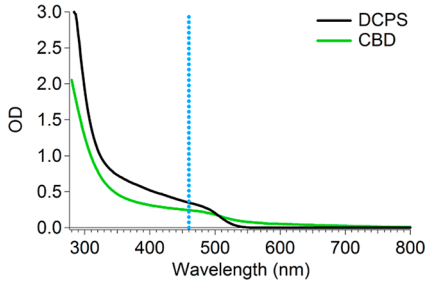

Figure 3. UV−vis absorption spectrum of CdS thin films coated on glass by DC pulse sputtering (DCPS), solid line, and chemical bath deposition (CBD), dotted line. The vertical broken line at 460 nm indicates the laser line used to excite the samples during transient absorption experiments.

(2.55 eV) which is consistent with the free electron absorption energy of bulk CdS.[29] Also shown in Figure 3 is the laser line used to excite the CdS samples during the TA measurements.

3.3. Transient Absorption Spectroscopy. The transient differential absorption (dA) spectra were recorded using a 460 nm pump and white light probe (450−800 nm) for the DCPS and CBD samples over the interval from 0 to 1000 ps delay between the pump and probe pulses. The wavelength dependent transient absorption (excited state absorption) and transient bleach (ground state depletion) recoveries were visualized by a 3D plot reported in Figure 4A/C for the two samples, respectively, and a 2D topographical plot shown in Figure 4B/C. The DCPS sample has a transient absorption feature at 450−470 nm, which did not fully recover to zero over the pump probe delay interval examined. There was also an asymmetric Gaussian transient bleach feature with λ_{max} = 510 nm, which recovered a majority of its amplitude within the pulse-width limited rise and 100 ps, with a fraction of the amplitude persisting through the remainder of the delays recorded. The CBD sample has a strong transient absorption feature below 450 nm, with significant amplitude out to 1000 ps. The transient bleach in this sample was blue-shifted with respect to that of the DCPS sample and was an asymmetric Gaussian feature with a λ_{max} = 490 nm. The pulse-width limited rise of the transient bleach recovered a majority of its amplitude before 200 ps delay, the remainder of which extended out to 1000 ps. The bleach feature width was broadened in the CBD sample.

3.3.1. Single Wavelength Fitting. Single wavelength time profiles were extracted from the data shown above for the λ_{max} of the transient bleach feature and shown normalized in Figure 5 (510 and 490 nm for DCPS and CBD, respectively). From this plot, it is seen that the time profiles recover with a fast, medium, and slow time constant. The two samples show very similar recoveries and differ primarily in the amplitude of the middle lifetime component, with the CBD sample having a larger amplitude in this region.

The bleach recoveries were fit with a triple exponential function, eq 1. Both time profiles could be fit with lifetimes of 8, 65, and 980 ps. The fit results were also shown (red lines) in Figure 5. From the single wavelength fits, the difference is small between the two samples. While the CBD sample has a larger amplitude for the medium decay, direct assignments regarding exciton dynamics are quite challenging. The samples differ in synthesis method, crystalline phase, and oxygen content; a more complete analysis technique is required to extract spectroscopic features, which can help to elucidate the effects of these differences on the exciton recombination dynamics.

$$y(\lambda, t) = y_0 + \sum_{i=1}^{n} A_i(\lambda)\exp\left(\frac{-t}{\tau_i}\right) \quad (1)$$

3.3.2. SVD Global Fitting. For transient absorption utilizing continuum probes, rich time-dependent spectroscopic information can be obtained so long as the time and wavelength dependence of the data can be deconvoluted. The aims of doing so would be to obtain a single time constant for a given decay process which will have no wavelength dependence. This can be accomplished through the utilization of SVD to deconvolute the wavelength and time dependence of the data, eq 2. The result of this analysis is the generation of two matrices containing orthogonal wavelength and time dependent vectors as well as a diagonal matrix containing eigenvalues ($\mathbf{\Sigma}$). A number of basis vectors are selected which contain actual data and the remaining vectors containing noise are discarded. The time dependent vectors are then fit with a series of exponentials to obtain the wavelength independent time constants governing the recombination dynamics. Subsequently, the wavelength dependence of the initial amplitude for each exponential function is determined, resulting in what is referred to as the B spectra.

$$\mathbf{M} = \mathbf{U\Sigma V}^* \quad (2)$$

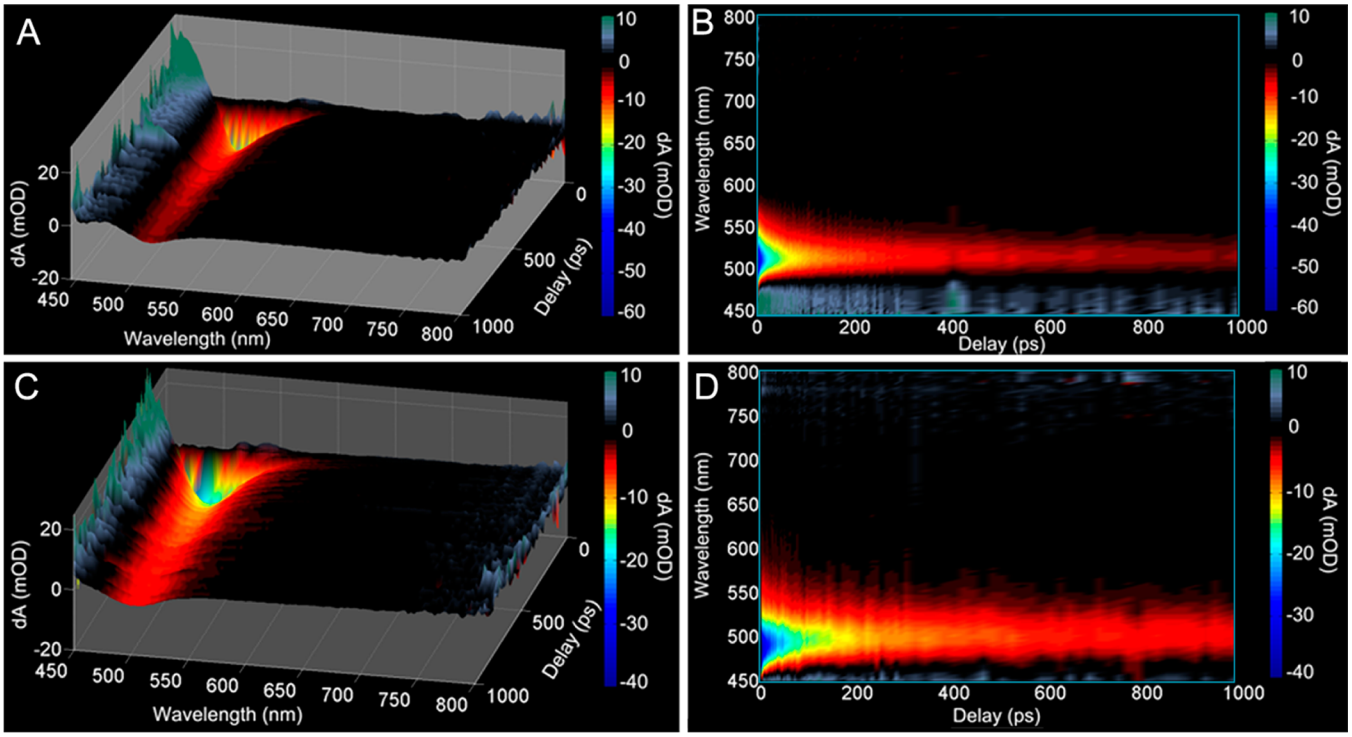

Figure 4. Transient absorption differential absorption spectrum of CdS thin films deposed on glass by DCPS (A/B) and CBD (C/D) covering 1000 ps pump probe delay for wavelengths between 450 and 800 nm displayed in 3/4 (A/C) and top down (B/D) views. Pump = 460 nm.

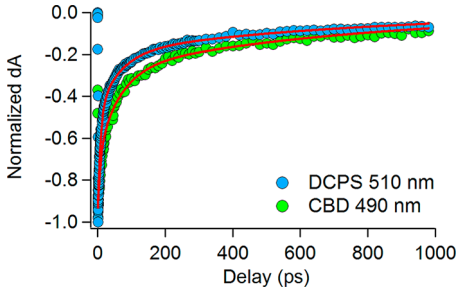

Figure 5. Normalized time dependence of the differential absorption for CdS thin films deposited by DCPS (blue) and CBD (green) circles for probe wavelengths 510 nm (DCPS) and 490 nm (CBD) probe. Triple exponential fit results are displayed as solid red lines. Fit lifetimes were 8, 65, and 980 ps.

While determining the lifetime of a given process can be a valuable tool for understanding recombination processes, semiconductor dynamics are usually more complicated than an ideal two-level system and thus often have multiexponential recoveries which can be difficult to assign to a specific transition. A greater depth of understanding can be gained from examining the wavelength dependent initial amplitude of each lifetime component for transient absorption, or the photon flux for time-resolved fluorescence techniques. We have successfully applied this analysis technique to study ZnSe:Cu,[30] core/shell/shell CdSe/ZnSe/ZnS,[31] and alloyed $Cd_xZn_{(1-x)}Se$/ZnSe/ZnS[32] systems to deconvolute time-resolved fluorescence and transient absorption peaks into separate spectral components which decay with single exponential lifetimes, thereby allowing for a more detailed discussion of the exciton recombination pathways associated with each lifetime component. Additional discussion on the SVD procedure is provided in the Supporting Information.

From the SVD deconvolution procedure, an orthogonal time dependence trace was obtained which was fit with a four exponential function (eq 1) for the DCPS sample and a triple exponential function for the CBD sample. Starting with the DCPS sample, the lifetimes were found to be 1.8 ± 0.2, 8 ± 0.5, 65 ± 3, and 450 ps. The longest time constant is not an accurate lifetime, as data was collected to 1 ns, which is not long enough to accurately fit the time dependence of this component. It is worth noting that the 1.8 ps lifetime was not necessary when the data was fit for a single wavelength of 510 nm but turns out to be an important component in the recombination (this point will be discussed in more detail later). The CBD sample was fit with lifetimes of 6 ± 0.4, 65 ± 3, and 450 ps. The lifetimes were independent of the pump flux. An example of the fit result for the DCPS sample excited with 220 nJ $pulse^{-1}$ is shown in Figure 6A, and the CBD sample excited with 195 nJ $pulse^{-1}$ in Figure 6C, in which the wavelength dependent initial amplitude (B spectra) for the lifetimes as well as the sum of four B spectra is given. For comparison, the raw data is also shown at six different pump probe time delays from 0.6 to 500 ps (colored as solid traces of decreasing gray densities outlined in black, respectively).

For the DCPS sample, the global fitting uncovered a 484 nm centered 1.8 ps component, which was missed in the single wavelength fitting as its amplitude at 510 nm is relatively low. This feature is more easily seen in the 2D topographical plot, Figure 6B, in which the 1.8 ps component is mixed with the chirp (substrate response) and appears to have a time-dependent red shift. The observation of a spectral red shift on this time scale is consistent with previous reports.[33] The 8 ps time constant (λ_{max} = 507 nm) is blue-shifted of the 65 ps component (λ_{max} = 509 nm), which decays monochromatically to the 450 ps component.

dx.doi.org/10.1021/am4018362 | ACS Appl. Mater. Interfaces 2013, 5, 7544−7551

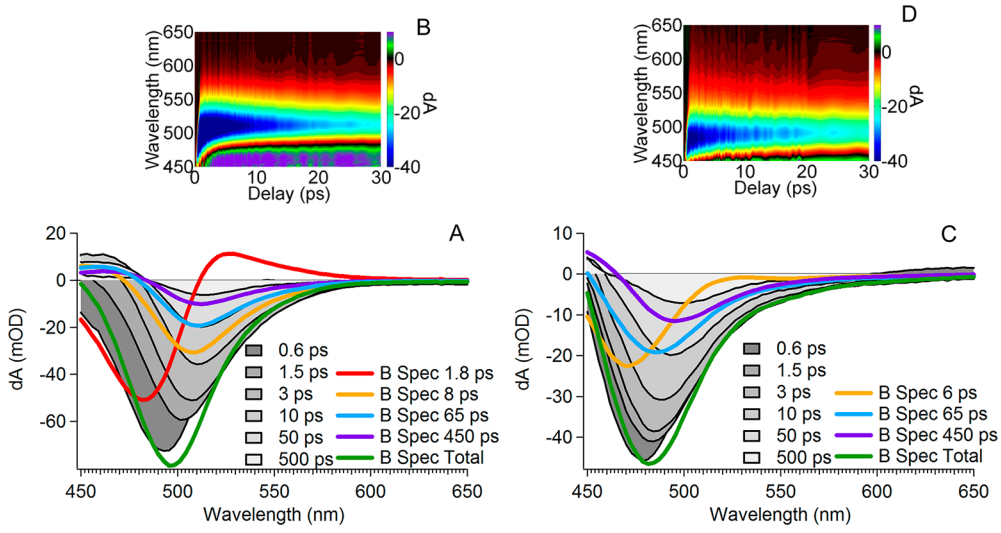

Figure 6. Example of SVD fit results for DCPS (A), 220 nJ pulse^{-1}, and CBD (C), 195 nJ pulse^{-1}, B spectra showing the wavelength dependence of initial amplitude of the various time constants. Also shown is the sum total of the B spectra (green). The raw data at a number of different time delays is also shown as solid traces of decreasing fill density from early to long delays. The raw topographical plots of the d*A* recovery over the first 30 ps are shown in B/D, respectively, for reference.

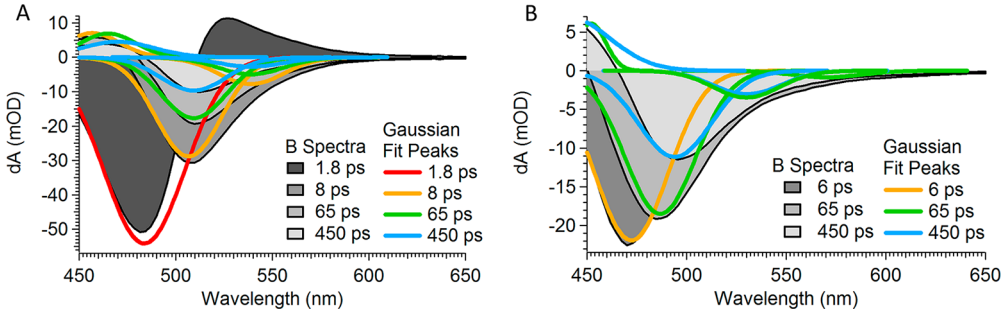

Figure 7. Singular value decomposition global fit of CdS DCPS (A) and CBD (B) thin film d*A* spectrum of various time constants (solid traces of decreasing black density from fast to slow). Multipeak Gaussian fits of each B spectra are shown as solid lines colored as follows: red, orange, green, and blue.

The CBD sample has a 6 ps (λ_{max} = 470 nm) feature, which in the topographical plot has less spectral red shift than the DCPS sample over the same 0−3 ps time interval. This can also be seen in the topography plot Figure 6D. The 65 ps component (λ_{max} = 484 nm) decays to a 450 ps component (λ_{max} = 493 nm). All CBD sample components were blue-shifted relative to the DCPS sample but had similar lifetimes. The discussion regarding the origin of these signals is continued below.

Further analysis of the B spectra was performed in an attempt to divide their broad asymmetric features by fitting each with a series of Gaussian peaks. The fit results for the DCPS (220 nJ pulse^{-1}) and CBD samples (195 nJ pulse^{-1}) were presented in Figure 7A and B, respectively, in which the B spectra for the various time constants are shown as solid traces decreasing in black density from fast to slow and outlined in solid black.

The Gaussian peaks used to fit the 1.8, 8, 65, and 450 ps B spectra are shown as red, orange, green, and blue traces, respectively.

For the DCPS sample, the B spectra have three major bleach components at 484, 507, and 539 nm. The 484 nm peak has a lifetime of 1.8 ps which decays to the two 507 and 539 nm peaks. The 507 nm peak has a lifetime of 8 ps and red shifts to a 509 nm peak, which decays monochromatically via two lifetimes of 65 and 450 ps without a spectral shift. The 539 nm peak decays triple exponentially with lifetimes of 8, 65, and 450 ps. There were also several excited state absorption features seen in the DCPS sample. The broad positive 1.8 ps feature starting at 530 nm and extending to the red is due to the chirp (substrate response) feature, which is partially mixed with this component toward the red wavelengths. The blue transients are seen in the 8, 65, and 450 ps lifetimes, but their λ_{max} could not be determined.

There were four significant CBD B spectra Gaussian fit peaks, the first of which was at 473 nm and has a lifetime of 6 ps. The following dominant feature at 486 nm decayed with a lifetime of 65 ps to a red-shifted peak at 494 nm with a 450 ps lifetime. Two smaller contributions to the B spectra were found at 530 nm, which have lifetimes of 65 and 450 ps. There was a remaining peak at 570 nm, which decayed with time constants of 65 and 450 ps. Excited state absorption was also seen in this sample, which extended blue of 465 nm with time constants of 65 and 450 ps.

The blue positive transients in both samples are assigned to a photoexcited electron trapped in a shallow or deep donor state being excited again by the probe to higher levels in the valence band (VB). This assignment is made because the recovery of these features mirrors the recovery of the donor related recovery, as discussed in more detail later.

dx.doi.org/10.1021/am4018362 | ACS Appl. Mater. Interfaces 2013, 5, 7544−7551

Each of the major Gaussian bleach features were plotted against the steady state UV−vis absorption spectrum for the DCPS and CBD samples, Figure 8. From this plot, it is clear

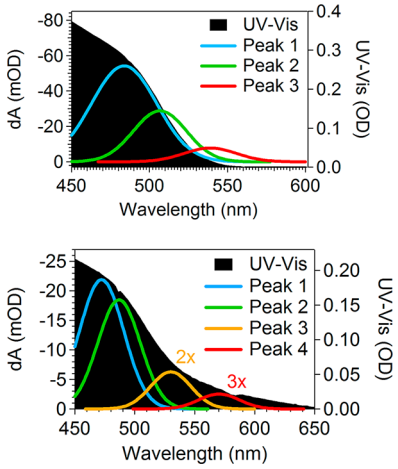

Figure 8. UV−vis spectrum (solid black) of the DCPS (top) and CBD (bottom) with the multi Gaussian fit peaks of the B spectrum for 220 and 195 nJ pulse $^{-1}$, respectively. Multipliers applied to peaks 3 and 4 are shown to improve comparisons.

that "peak 1" for the DCPS sample is the first exciton absorption for CdS. The following peaks 2 and 3 describe the exponential decay of the absorption spectra, the Urbach tail.

The CBD sample peak 1 is blue-shifted compared to E_g while peak 2 is due to the first exciton absorption. The origin of the blue-shifted peak 1 is discussed below. The Urbach tail for this sample, described by peaks 3 and 4, is much broader than in the DCPS sample. The broad absorption tail is consistent with an amorphous material rich defect level absorption,[34] herein ascribed to O_i and V_S states. We attribute peak 3 to absorption from CB to acceptor levels, while peak 4 is attributed to absorption from associated centers of O_i acceptor to V_S donor states.

It should be made clear that a transient bleach feature found in the d*A* spectrum is related to depopulation of the ground state. For CdS, E_g is 2.55 eV as seen in Figure 8. The DCPS sample 1.8 ps lifetime component with a spectral peak at 484 nm (2.56 eV) is assigned the trapping rate of photoelectrons from CB to shallow and deep donor levels. The peak found at 507 nm (2.45 eV) which decays with an 8 ps lifetime represents a ∼100 meV energy difference between the E_g energy. The peak at 539 nm (2.30 eV) is 240 meV less than the E_g. Because both of these peaks are transient bleach features, reduced absorption to or from these transitions was caused by stimulation of the sample by the pump. It is suggested that the 2.45 eV peak is due to an excitation from the VB to a shallow donor state and the 2.30 eV peak is due to a excitation from the VB to a deep donor. Increased electron density in donor states produced by excitation of VB electrons to the CB and subsequent decay to these donor states would cause increased state filling and decreased absorption to these states from VB → donor excitation. Therefore, the CB → donor, CB → VB, shallow donor → VB, and deep donor → VB translations are governed by lifetimes of 1.8, 8, 65, and 450 ps, respectively.

The CBD sample peak at 473 nm (2.62 eV) represents absorption from the VB → CB, which at early delay times is blue-shifted with respect to the expected E_g (2.55 eV). This is caused from a high donor density in the sample, which in turn overpopulates the CB with electrons upon photoexcitation by the pump, resulting in state filling and a shift in the apparent forbidden gap. The following peak at 486 nm (2.55 eV) is related to the decreased VB → CB absorption after the overpopulated CB empties into donor states below the CB. The peak at 530 nm (2.34 eV) is E_g − 210 meV and is attributed to the VB → acceptor excitation. The remaining 570 nm peak (2.17 eV) is E_g − 380 meV which is due to acceptor to donor transitions. The acceptor level is associated with O_i and the donor levels are due to V_S. The increased V_S is attributed to O doping.

The above-described transitions and recombination processes have been summarized in Figure 9 and refer specifically

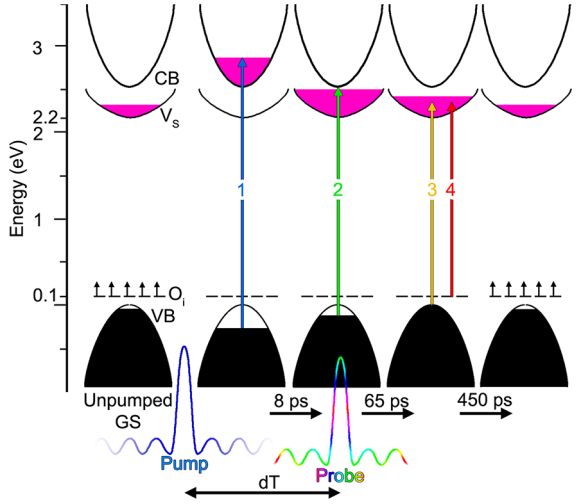

Figure 9. Mechanism of electron relaxation investigated by ultrafast pump probe spectroscopy stimulated by 460 nm pump and probed with white light (450−800 nm) continuum for the CBD sample. Electrons in the unpumped ground state (GS) occupy the VB and partially both O_i acceptor and V_S donor states. Excitation with the pump laser depopulates the electrons, which decay back to the ground state via three lifetimes: 8, 65, and 450 ps. The vertical transitions detail the origin of the observed features in the d*A* spectrum for this sample. Labels 1−4 refer to the peak assignments made in Figure 8. The relative occupation density of the CB and V_S and depopulation of VB electrons (solid pink and black, respectively) are used as a visual tool and are not to be taken precisely.

to the CBD dynamics. The unpumped sample has a partially depopulated CB due to O_i acceptor states, while the V_S donor states are partially filled at room temperature. Upon excitation by the pump pulse, electrons are depopulated from both O_i and V_S states as well as the VB to fill the CB. For early time delays, the CB → VB transitions are blue-shifted due to state filling. After 1−2 ps, electrons repopulate the V_S states causing a red shift of the VB → CB transition. The remaining signals observed in the TA spectrum are due to depopulated acceptor state transitions to either donor levels or CB. A number of recombination channels are possible involving the V_S electrons. The first 8 ps decay is assigned to recombination from CB → VB. The 65 ps recombination can be attributed to V_S to CB decay with the remaining 450 ps component due to V_S to O_i recombination.

3.3.3. Power Dependence. The TA d*A* spectrum was recorded for each sample under five different pump fluences ranging from 24, 48, 86, 220, and 707 nJ pulse^{-1} for the DCPS

dx.doi.org/10.1021/am4018362 | ACS Appl. Mater. Interfaces 2013, 5, 7544−7551

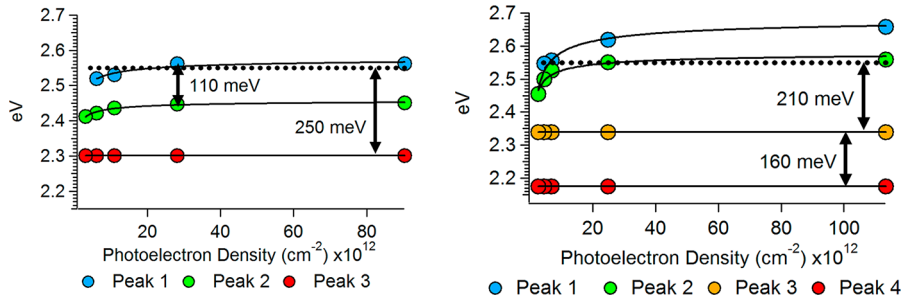

Figure 10. Plot of the laser pump induced photoelectron density vs λ_{max} of the DCPS (left) and CBD (right) B spectra Gaussian fit features. Peak labels are with respect to Figure 8 assignments. Data fits are shown as solid lines.

sample and 20, 35, 54, 195, and 890 nJ pulse^{-1} for the CBD sample. The TA spectra were analyzed with the above-described SVD-global fitting methodology, and the resulting B spectra were reported in Supporting Information Figure S3. Considering the optical density of the substrate and the laser spot area (1 mm^2), the electron hole density created upon photo excitation (η) ranged from 2.5×10^{12} to 1.1×10^{14} cm^{-3}. These densities are well below the Mott criterion ($\eta \sim a_B^{-3}$), where a_B is the Bohr exciton radius, for significant exchange correlation effects and subsequent bandgap renormalization effects.[35] All decay components for both samples showed linear power dependence of the dA amplitude; the fast component amplitude was presented in Supporting Information Figure S4 for both DCPS and CBD samples.

The power dependence of the λ_{max} of the B spectra Gaussian fit peaks for the two samples are shown in Figure 10. The following "peak" labels refer to Figure 8 labels and have been colored, respectively.

Beginning with the DCPS sample, 1.8 ps B spectrum Gaussian fit peak 1 had no amplitude at 24 nJ pulse^{-1} pump fluence but increased with an inverse square root dependence from 2.52 to 2.56 eV from 48 to 707 nJ pulse^{-1}, respectively. The observed E_g in the dA spectrum crossed the expected first exciton absorption energy slightly above the 86 nJ pulse^{-1} pump energy (1.1×10^{13} cm^{-3} photoelectron density). The 8 ps time constant B spectra had two Gaussian fit peaks. The first peak 2 had an absorption energy of 2.41 eV at 24 nJ pulse^{-1} and increased with an inverse square root dependence to 2.45 eV at 707 nJ pulse^{-1}. The E_g offset of this peak at 220 nJ pulse^{-1} was 110 meV. The second peak in the 8 ps B spectrum, peak 3, was pump power independent, which has an absorption energy of 2.3 eV. The E_g offset of this last peak was 250 meV. Low donor density and fast recombination lifetime of the CB → VB transition can explain the reduced Burstein−Moss shift in the DCPS sample. Considering the E_g offset and that they are bleach features, peaks 2 and 3 are assigned to a VB → donor level absorption. There are a number of donor states in CdS in this energy range, and little can be said about the identity of the states involved in the transitions.[10] Peak 2 was seen to have the same power dependent energy shift as peak 1. This indicates that a trapping process, lower in energy than peak 2, becomes saturated at higher powers and allows for state filling in both peak 1 and 2 bands.

For the CBD sample, the 6 ps B spectrum Gaussian fit has an absorption energy (peak 1) at the lowest excitation energy of 2.46 eV, which blue-shifted with an inverse square root dependence to 2.66 eV at 890 nJ pulse^{-1}. In the 65 ps B spectrum, there were three Gaussian features of majority contribution. The first peak, peak 2, started at 2.46 eV at the lowest pump power and blue-shifted to 2.56 eV at the highest pump power with inverse square root dependence as well. The second (peak 3) and third (peak 4) peak positions are power independent at 2.34 eV (530 nm) and 2.18 eV (570 nm), respectively. The lack of any power dependence of the latter two peaks is consistent with the assignment of these features due to CB → V_S and O_i → V_S absorption, as seen in the dA spectrum, respectively. Also, the significant shift of the apparent gap in the peak 1 data suggests the donor density in the CBD sample was higher than the DCPS sample. Due to the expected donor level of the V_S states, peak 4 is consistent with a VB → V_S transition. The remaining peak 4 is assigned to DAP absorption between O_i → V_S.

4. CONCLUSIONS

The exciton dynamics in CdS thin films prepared by DC pulse sputtering (DCPS) and chemical bath deposition (CBD) have been studied by ultrafast transient absorption pump probe spectroscopy. The DCPS film of 100 nm thickness consists of the wurtzite crystalline phase, while the CBD sample of 70 nm thickness of the zinc blende phase of lower crystallinity than the DCPS sample. The oxygen content in the CBD sample was taken to be approximately 10%. The differential absorption (dA) was monitored by a while light probe for the first 1 ns after photoexcitation by a 460 nm pump at five different excitation fluence. SVD global fitting was applied to the dA spectra to obtain wavelength independent lifetimes and time independent initial amplitudes (B spectra). The lifetimes of the DCPS sample were 1.8, 8, 65, and 450 ps which were related to carrier trapping in donor states, CB → VB recombination, shallow donor recombination, and deep trap recombination, respectively. The CBD sample has lifetimes of 6, 65, and 450 ps which were assigned to CB → VB recombination, donor → VB recombination related to V_S states, and donor−acceptor pair (DAP) recombination due to V_S → O_i, respectively. Detailed analysis of the B spectra supports the above assignments and was compared for the range of pump fluence used. The results suggest that DCPS deposited CdS should provide improved performance in applications such as window layers in solid state solar cells. This study also demonstrates the power of ultrafast laser spectroscopy in unraveling detailed information about exciton and charge carrier dynamics in semiconductors.

■ ASSOCIATED CONTENT

Supporting Information

Singular value decomposition details as well as Figures S1−S4 as mentioned in the text. This material is available free of charge via the Internet at http://pubs.acs.org.

AUTHOR INFORMATION

Corresponding Author

*Phone. 831-459-3776. E-mail: zhang@ucsc.edu (J.Z.Z.); caoj@ge.com (J.C.).

Notes

The authors declare no competing financial interest.

ACKNOWLEDGMENTS

This work was supported by the BES Division of the US DOE. The authors gratefully appreciate Yashar Abdollahian for his expertise and time in collecting XRD. Special thanks to Tom Yuzvinsky for his assistance with SEM. Thanks to Robert Fitzmorris for helpful discussion and editing.

REFERENCES

(1) Chirilă, A.; Buecheler, S.; Pianezzi, F.; Bloesch, P.; Gretener, C.; Uhl, A. R.; Fella, C.; Kranz, L.; Perrenoud, J.; Seyrling, S.; Verma, R.; Nishiwaki, S.; Romanyuk, Y. E.; Bilger, G.; Tiwari, A. N. *Nat. Mater.* **2011**, *10*, 857−861.

(2) Oliva, A.; Castro-Rodrıguez, R.; Solıs-Canto, O.; Sosa, V. c.; Quintana, P.; Pena, J. *Appl. Surf. Sci.* **2003**, *205*, 56−64.

(3) Martil, I.; Diego, N. D.; Hidalgo, C. *Phys. Stat. Sol. A* **1986**, *94*, 587−593.

(4) Kadirgan, F.; Mao, D.; Song, W.; Ohno, T.; McCandless, B. *Turk. J. Chem.* **2000**, *24*, 21−34.

(5) El Deeb, A. F. *Eur. Phys. J.−Appl. Phys.* **2007**, *38*, 247−252.

(6) Vigil-Galán, O.; Vidal-Larramendi, J.; Escamilla-Esquivel, A.; Contreras-Puente, G.; Cruz-Gandarilla, F.; Arriaga-Mejía, G.; Chavarría-Castañeda, M.; Tufiño-Velázquez, M. *Phys. Stat. Sol. A* **2006**, *203*, 2018−2023.

(7) Escamilla-Esquivel, A.; Contreras-Puente, G.; Tufino-Velazquez, M.; Albor-Aguilera, M.; Vigil, O.; Vaillant, L. *J. Appl. Phys.* **1999**, *86*, 3171−3174.

(8) Raji, P.; Sanjeeviraja, C.; Ramachandran, K. *Bull. Mater. Sci.* **2005**, *28*, 233−238.

(9) Taguchi, T.; Ray, B. *Prog. Cryst. Growth Charact. Mater.* **1983**, *6*, 103−162.

(10) Abken, A. E.; Halliday, D.; Durose, K. *J. Appl. Phys.* **2009**, *105*, 064515−064515−9.

(11) Aguilar-Hernández, J.; Contreras-Puente, G.; Morales-Acevedo, A.; Vigil-Galán, O.; Cruz-Gandarilla, F.; Vidal-Larramendi, J.; Escamilla-Esquivel, A.; Hernández-Contreras, H.; Hesiquio-Garduño, M.; Arias-Carbajal, A.; Chavarría-Castañeda, M.; Arriaga-Mejía, G. *Semicond. Sci. Technol.* **2003**, *18*, 111.

(12) Wenyi, L.; Xun, C.; Qiulong, C.; Zhibin, Z. *Mater. Lett.* **2005**, *59*, 1−5.

(13) Subba Ramaiah, K.; Pilkington, R. D.; Hill, A. E.; Tomlinson, R. D.; Bhatnagar, A. K. *Mater. Chem. Phys.* **2001**, *68*, 22−30.

(14) Espinosa-Rosas, M.; Aguilar-Hernández, J.; Hernández-Contreras, H.; Hernández-Pérez, M.; Contreras-Puente, G.; Cárdenas-García, M.; Ortega-Nájera, B. *Mater. Sci. Forum* **2011**, *691*, 145−150.

(15) Gutowski, J.; Sebald, K.; Voss, T. CdS: ionization energies (impurities and defects). In *Landolt-Bornstein: Semiconductors—New Data and Updates for II−VI Compounds*; Rossler, U., Ed.; Springer-Verlag: Berlin Heidelberg, Germany, 2008; Vol. *III/44B*.

(16) Rempel, A. A.; Valeeva, A. A.; Kozhevnikova, N. S. *JETP Lett.* **2010**, *92*, 146−150.

(17) Kar, S.; Biswas, S.; Chaudhuri, S.; Nambissan, P. M. G. *Phys. Rev. B* **2005**, *72*, 075338.

(18) O'Brien, P.; McAleese, J. *J. Mater. Chem.* **1998**, *8*, 2309−2314.

(19) Kylner, A.; Lindgren, J.; Stolt, L. *J. Electrochem. Soc.* **1996**, *143*, 2662−2669.

(20) Stoev, M.; Katerski, A. *J. Mater. Chem.* **1996**, *6*, 377−380.

(21) Yandong, M.; Dai, Y.; Huang, B. *Comput. Mater. Sci.* **2011**, *50*, 1661−1666.

(22) Chadi, D. J. *Annu. Rev. Mater. Sci.* **1994**, *24*, 45−62.

(23) Akimoto, K.; Okuyama, H.; Ikeda, M.; Mori, Y. *J. Cryst. Growth* **1992**, *117*, 420−423.

(24) Akimoto, K.; Okuyama, H.; Ikeda, M.; Mori, Y. *Appl. Phys. Lett.* **1992**, *60*, 91−93.

(25) Nazarova, L. D.; Morozova, N. K.; Butnev, K. N. *Inorg. Mater.* **1996**, *32*, 481−484.

(26) Zhong, D.; Parthasarathy, G.; Nardi, R. A. *Photovoltaic device and method for making*. U.S. Patent 8044477, 2011.

(27) Newhouse, R. J.; Wang, H.; Hensel, J. K.; Wheeler, D. A.; Zou, S.; Zhang, J. Z. *J. Phys. Chem. Lett.* **2011**, *2*, 228−235.

(28) Hug, S. J.; Lewis, J. W.; Einterz, C. M.; Thorgeirsson, T. E.; Kliger, D. S. *Biochemistry* **1990**, *29*, 1475−1485.

(29) Gutowski, J.; Sebald, K.; Voss, T. CdS: exciton energies, exciton binding energies. In *Landolt-Bornstein: Semiconductors—New Data and Updates for II−VI Compounds*; Rossler, U., Ed.; Springer-Verlag: Berlin Heidelberg, Germany, 2008; Vol. *III/44B*.

(30) Gul, S.; Cooper, J. K.; Corrado, C.; Vollbrecht, B.; Bridges, F.; Guo, J.; Zhang, J. Z. *J. Phys. Chem. C* **2011**, *115*, 20864−20875.

(31) Fitzmorris, B. C.; Cooper, J. K.; Edberg, J.; Gul, S.; Guo, J.; Zhang, J. Z. *J. Phys. Chem. C* **2012**, *116*, 25065−25073.

(32) Fitzmorris, B. C.; Pu, Y.-C.; Cooper, J. K.; Lin, Y.-F.; Hsu, Y.-J.; Li, Y.; Zhang, J. Z. *ACS Appl. Mater. Interfaces* **2013**, *5*, 2893−2900.

(33) Logunov, S.; Green, T.; Marguet, S.; El-Sayed, M. A. *J. Phys. Chem. A* **1998**, *102*, 5652−5658.

(34) John, S.; Soukoulis, C.; Cohen, M. H.; Economou, E. *Phys. Rev. Lett.* **1986**, *57*, 1777−1780.

(35) Grundmann, M. *The Physics of Semiconductors: An Introduction Including Devices and Nanophysics*; Springer-Verlag: Berlin Heidelberg, Germany, 2006.